BATTERIES

Capturing the swelling of solid-electrolyte interphase in lithium metal batteries

Zewen Zhang[1], Yuzhang Li[1,2], Rong Xu[1], Weijiang Zhou[3], Yanbin Li[1], Solomon T. Oyakhire[4], Yecun Wu[5], Jinwei Xu[1], Hansen Wang[1], Zhiao Yu[4,6], David T. Boyle[6], William Huang[1], Yusheng Ye[1], Hao Chen[1], Jiayu Wan[1], Zhenan Bao[4], Wah Chiu[3,7,8]*, Yi Cui[1,9]*

Although liquid-solid interfaces are foundational in broad areas of science, characterizing this delicate interface remains inherently difficult because of shortcomings in existing tools to access liquid and solid phases simultaneously at the nanoscale. This leads to substantial gaps in our understanding of the structure and chemistry of key interfaces in battery systems. We adopt and modify a thin film vitrification method to preserve the sensitive yet critical interfaces in batteries at native liquid electrolyte environments to enable cryo–electron microscopy and spectroscopy. We report substantial swelling of the solid-electrolyte interphase (SEI) on lithium metal anode in various electrolytes. The swelling behavior is dependent on electrolyte chemistry and is highly correlated to battery performance. Higher degrees of SEI swelling tend to exhibit poor electrochemical cycling.

Electrode-electrolyte interfaces are important to technologies ranging from electrical energy generation and storage to the synthesis of chemicals and materials (*1*, *2*). These electrochemical interfaces are complex and experimentally difficult to study, in part as the result of a lack of effective tools to characterize with high resolution. This gap in understanding has contributed to insufficient experimental control over interfacial structure and reactivity. For example, the solid-electrolyte interphase (SEI)—an interfacial layer formed at the electrode-electrolyte interface because of the electrochemical and chemical decomposition of electrolytes—is a key component responsible for the reversible operation of Li-ion and Li metal batteries (*3*–*5*). Thus, efforts have been made to engineer the SEI to enable battery chemistries with higher energy densities and longer cycles (*6*–*9*). However, fundamental understanding of the interfacial phenomena in these battery chemistries is still limited. Elucidating the nanoscale structures and chemistries at the electrode-electrolyte interface is therefore critical for developing high–energy density batteries (*10*–*13*).

Conventional characterization techniques with high spatial resolution, such as high-resolution transmission electron microscopy (HRTEM), are incompatible with volatile liquid electrolytes and sensitive solid electrodes, like Li metal anode. Moreover, both electrodes and electrolytes are highly reactive and easily subject to contamination or damage during sample preparation and transfer. Cryogenic temperatures can help stabilize sensitive battery materials and interfaces during sample preparation and enable high-resolution characterization in TEM (*14*–*18*). Nonetheless, the nanoscale structure of SEI in the layer that is closely interfaced with the electrode revealed with cryo–electron microscopy (cryo-EM) in many state-of-the-art electrolytes is often amorphous (*6*, *7*). Thus, it is hard to correlate the difference in battery performance with the SEI nanostructure and chemistry.

The experiments referenced in the previous paragraph were performed in the absence of liquid electrolyte; however, ideally one would want to preserve the solid-liquid interface in the "wet" state with liquid electrolyte. A cryo–scanning transmission electron microscopy (cryo-STEM) method, combined with cryo–focused ion beam (cryo-FIB), was reported to access the buried interface in batteries with solid and liquid phases together (*19*). However, high-resolution imaging of SEI in the electrolyte is difficult because of the technical challenge in preparing thin enough lamellae suitable for HRTEM. Additionally, the effect of ion milling on SEI nanostructure and chemistry is also a concern.

We adapt the original thin film vitrification method (*20*) to preserve the electrode-electrolyte interface of batteries in its native organic liquid electrolyte environment. Such samples can be characterized with cryo-(S)TEM to investigate the intact structure and chemistry of the interphase in Li metal batteries. The key is to directly obtain thin film specimens of organic liquid electrolyte interfaced with the solid battery material while avoiding any mechanical or chemical artifacts from extra sample preparation steps.

Figure 1, A and B, shows a schematic of the thin film vitrification method developed for batteries and the cross-sectional view of the vitrified specimen. Such a process yields uniform thin films inside the holes throughout the grid (fig. S1) and generates the electron-transparency of the specimen (fig. S2, A to C). There are two crucial factors to ensure that the vitrification of organic electrolytes is a practical method. (i) Organic solvent molecules often require substantially slower cooling rates for vitrification than aqueous solutions of biological samples (*21*), so the original method of freezing biological specimens directly in liquid nitrogen was used. (ii) Although lower in surface tension, organic electrolytes can still form a self-supporting thin film of submicron thickness by themselves and can remain for seconds before breaking as aqueous solutions. The amorphous diffraction pattern of pure frozen electrolyte without any salt or solvent crystallization confirms the successful vitrification process (fig. S2, D and E). Cryo–scanning electron microscopy (cryo-SEM) revealed rod-shape morphologies covered by a thin film in the TEM grid hole, corresponding to Li metal dendrites covered with a thin layer of vitrified electrolyte (Fig. 1, D and E, and fig. S2, F and G).

Li metal plated in commercial carbonate electrolyte—1 M $LiPF_6$ in ethylene carbonate/diethyl carbonate (EC/DEC)—was used as an example to reveal the SEI in the electrolyte. In Fig. 2A, Li metal dendrites show a lighter contrast compared with that of the organic electrolyte as a result of a lower average atomic number. A thick layer of ~20 nm with slightly darker contrast in the vitrified electrolyte was identified as the SEI layer (Fig. 2C). However, the SEI characterized in the absence of liquid electrolyte is ~10 nm thick (Fig. 2D). There is a visible thickness difference between these two samples (Fig. 2E) that can be observed across multiple experiments (Fig. 2F). A video recorded after electrolyte removal but without drying shows that the SEI shrinks under electron beam exposure as a result of the evaporation of volatile solvent species (movie S2). Thus, this change in thickness should be ascribed to the loss of electrolyte species during washing and drying in preparing dry-state samples, which indicates a swollen SEI in the electrolyte environment. In the following discussion, the SEI in the electrolyte is denoted as w-SEI to indicate that the SEI is in a vitrified (also referred to as a wet or w-) state, and the SEI in the absence of electrolyte is denoted as d-SEI to indicate that the SEI is in a dry state.

We used cryo-STEM and electron energy-loss spectroscopy (EELS) to explore the chemistry

[1]Department of Materials Science and Engineering, Stanford University, Stanford, CA 94305, USA. [2]Department of Chemical and Biomolecular Engineering, University of California Los Angeles, Los Angeles, CA 90095, USA. [3]Biophysics Program, School of Medicine, Stanford University, Stanford, CA 94305, USA. [4]Department of Chemical Engineering, Stanford University, Stanford, CA 94305, USA. [5]Department of Electrical Engineering, Stanford University, Stanford, CA 94305, USA. [6]Department of Chemistry, Stanford University, Stanford, CA 94305, USA. [7]Department of Bioengineering, Stanford University, Stanford, CA 94305, USA. [8]Division of Cryo-EM and Bioimaging, SSRL, SLAC National Accelerator Laboratory, Menlo Park, CA 94025, USA. [9]Stanford Institute for Materials and Energy Sciences, SLAC National Accelerator Laboratory, Menlo Park, CA 94025, USA.
***Corresponding author. Email: wahc@stanford.edu (W.C.); yicui@stanford.edu (Y.C.)**

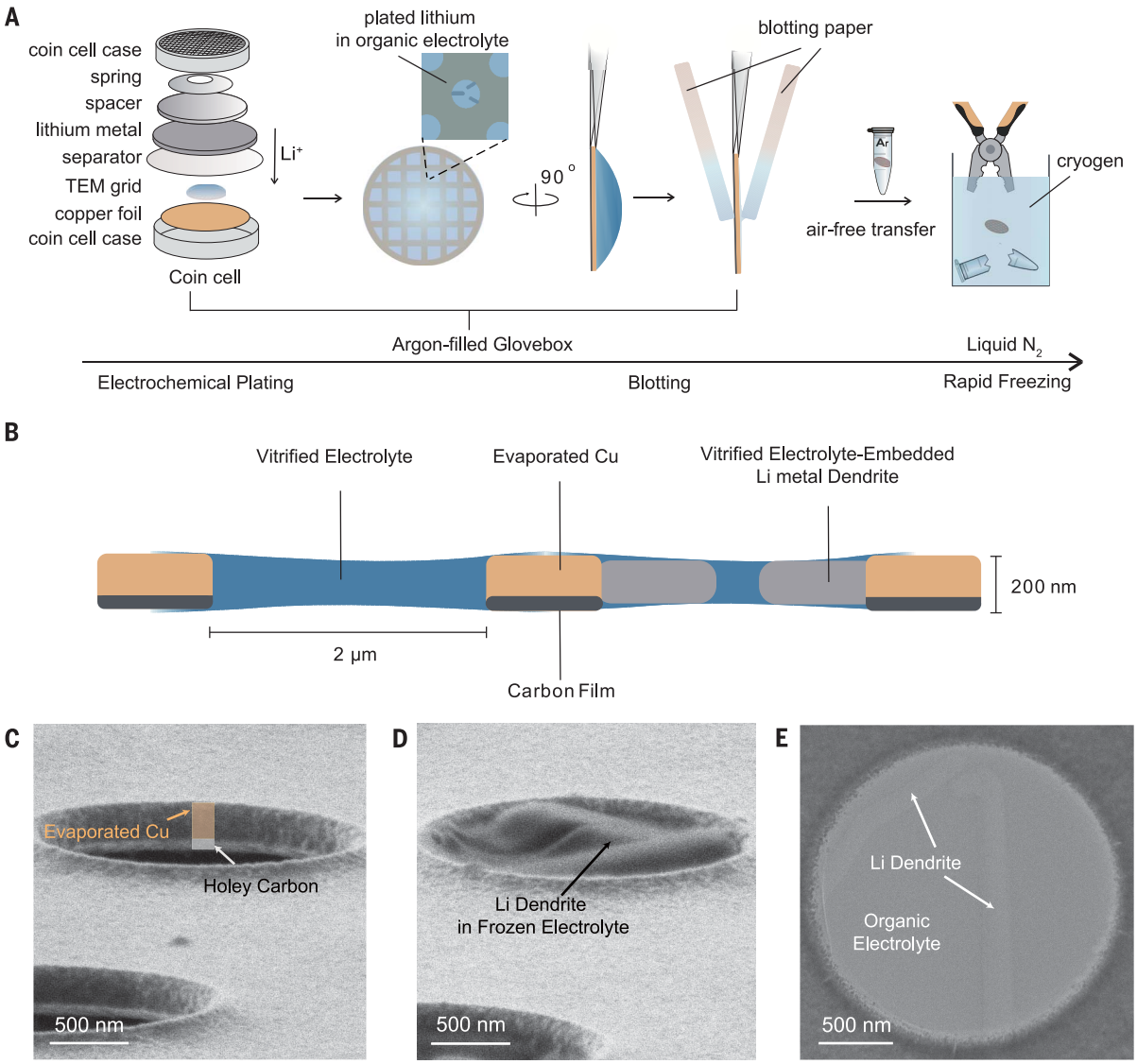

Fig. 1. Sample preparation of dendrite in vitrified organic electrolyte. (**A**) Schematic process of sample preparation for vitrified specimens. Cu-evaporated commercial holey carbon TEM grids were used as the working electrode for Li metal plating in the coin cell setup. Upon coin cell disassembly after Li metal deposition, excess electrolyte on the TEM grid is removed with double-sided blotting (movie S1) in an Ar-filled glove box and vitrified by liquid nitrogen without air exposure. (**B**) Schematic cross section of vitrified specimens. (**C**) Cryo-SEM image of Cu-evaporated TEM grid. (**D**) Cryo-SEM image of frozen Li metal dendrite along with electrolyte. (**E**) Cryo-TEM image of Li dendrite in frozen electrolyte. The light-contrast rodlike region represents the Li metal dendrite.

of Li metal and its SEI in vitrified electrolyte. Spectroscopic mapping of EELS shows that the SEI layer is tens of nanometers thick (fig. S4). We observe distinct carbon-bonding environments in the d-SEI, the w-SEI, and the electrolyte in the carbon K-edge fine structures (fig. S5). The peaks at 288 and 290 eV correspond to C–H and carbonate C=O bonds present in all three regions, consistent with evidence that SEI is mainly composed of alkyl carbonates in carbonate-based electrolyte (*22*). The increase in the relative intensity of C–H bonds from the w-SEI compared with the d-SEI correlates well with the observed swelling behavior. More carbonate-based organic molecules are present in the SEI layer in the wet state. Thus, the average carbon and oxygen bonding environment in the w-SEI more closely resembles that in the electrolyte as compared with the d-SEI.

Local mechanical properties of SEI were measured by nanoindentation with atomic force microscopy (AFM). The measurements were carried out in an inert environment to prevent undesired side reactions, and for w-SEI particularly, a closed liquid cell for AFM was used to further keep the electrode in the liquid electrolyte environment (fig. S6A). Typical force-displacement curves for nanoindentation experiments on both d-SEI and w-SEI are shown in Fig. 3. w-SEI showed an elastic-plastic deformation, where the force-displacement curves during loading and unloading are not fully reversible. However, under similar force loading, d-SEI only exhibited elastic deformation with small displacement (<5 nm) (fig. S6, C and D). The elastic modulus of w-SEI is 0.31 ± 0.14 GPa, whereas that of d-SEI is 2.01 ± 0.63 GPa. This difference can be explained by the swelling behavior of SEI in liquid electrolyte because swelling can cause polymers to soften (*23*). Additionally, swelling has been shown to increase the spatial heterogeneity of polymer materials (*24*), which corresponds to a more diverse distribution of elastic modulus from w-SEI.

Our result suggests that SEI is in a swollen state in liquid electrolyte. This is important in

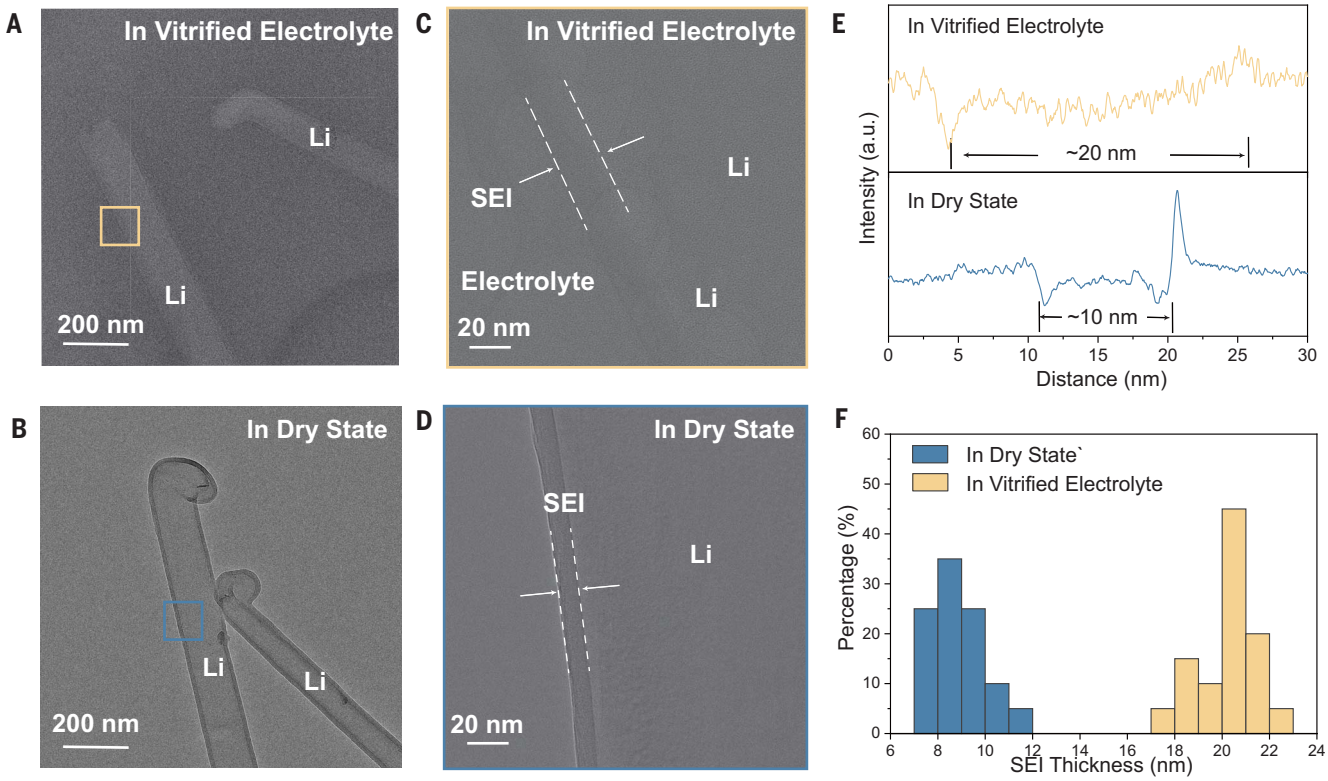

Fig. 2. SEI on Li dendrite in dry state and vitrified organic electrolyte imaged with cryo-TEM. (**A** and **B**) Li metal dendrites in vitrified electrolyte (A) and in dry state (B). (**C** and **D**) HRTEM of SEI on Li metal dendrite in vitrified electrolyte (C) and in dry state (D). (**E**) Representative line profiles of intensity across the interfaces on Li metal dendrite deposited in 1 M $LiPF_6$ in EC/DEC electrolyte. a.u., arbitrary units. (**F**) The histogram of SEI thickness in vitrified electrolyte and in dry state across multiple Li metal dendrites with 20 measurements for both in vitrified electrolyte and in dry state.

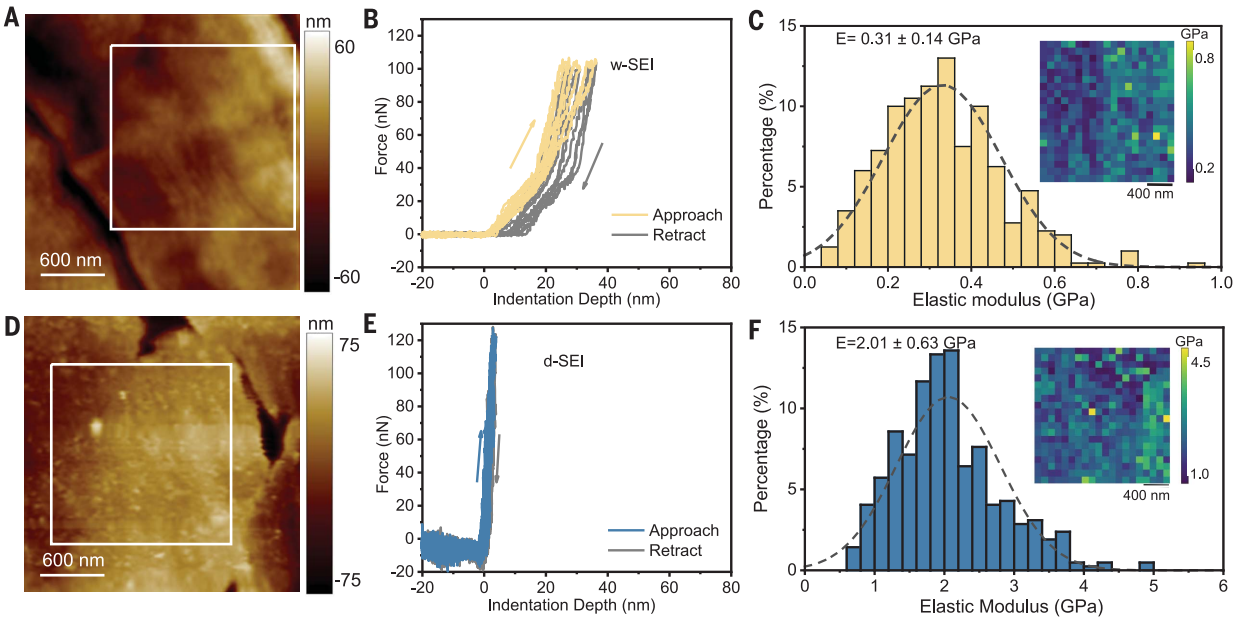

Fig. 3. AFM nanoindentation analysis of SEI in liquid electrolyte. (**A** and **D**) AFM height images of deposited Li metal in liquid electrolyte (A) and in dry state (D). The white box indicates the region for nanoindentation mapping. (**B** and **E**) Representative force-displacement curves for nanoindentation experiments for both w-SEI (B) and d-SEI (E). (**C** and **F**) Histograms of the elastic modulus of w-SEI (C) and of d-SEI (F). The insets are corresponding two-dimensional maps of elastic moduli in the regions of interest. Indentation displacement curves were offset for clarity. The scales of the *x* axes are different in (C) and (F).

part because it suggests that SEI may not be a dense layer and that there is a nontrivial amount of electrolyte in this region. This is different from previous understanding, where SEI was thought to be a mixing layer of solid inorganic species (such as Li_2O, Li_2CO_3, etc.) and polymers and thus was electrolyte blocking and surface passivating to make the electrode-electrolyte interface metastable. Our results indicate that the electrolyte is in close contact with the electrode at the solid-liquid interface in batteries. Several fundamental yet critical aspects about this interface, for example the Li-ion desolvation process and Li-ion transport mechanism through SEI, need to be reconsidered to better understand the key processes during battery cycling. Notably, after calendar aging or cycling, SEI can become much thicker, where the swelling might become more substantial and eventually lead to the drying out of the electrolyte (*25*, *26*).

Furthermore, the swelling of SEI sheds light on the mechanism of SEI growth after the formation of the initial SEI layer. Previously, the decrease in the rate of SEI formation was projected to be caused by the need for the reactants to diffuse through the already-existing layer (*27*). However, whether it is solvent diffusion through SEI inward to electrode surface or electron conduction through SEI outward toward electrolyte is still subject to debate. On the basis of our observation, it is highly likely that solvent diffusion plays a more significant role in the continuous growth of the SEI, particularly because the presence of solvents within the SEI reduces the distance required for electron tunneling during the decomposition of electrolytes. The reaction hotspot is now at or near the electrode-SEI interface.

This observation provides a practical method to quantitatively measure the electrolyte uptake of SEI in the liquid environment. Alternatively, this can also be viewed as SEI porosity at (sub)-nanoscale, as projected in earlier SEI models (*27*–*30*). By measuring the swelling ratio, defined as the thickness ratio of w-SEI and d-SEI, we can estimate the amount of electrolyte in the SEI region. For example, in 1 M $LiPF_6$ in EC/DEC, the w-SEI has an average thickness of 20 nm, whereas the d-SEI is ~10 nm. This indicates that ~50% of the SEI volume is composed of the electrolyte. Further questions, like nanoscale pore or electrolyte distribution in the SEI, need to be addressed for better understanding of the transport mechanism of Li across the interface.

SEI is the key determinant for Li metal anode performance, and its properties vary with electrolyte systems, where solvent chemistry and salt composition largely determine SEI composition and structure (*31*). Even changing salt concentration would alter the solvation chemistry and the derived SEI (*9*). Generally, a mechanically robust, spatially uniform, and chemically passivating SEI is desirable (*32*). The swelling of SEI directly contradicts these design principles. We hypothesize that a better SEI should swell less with the electrolyte.

As a test of the above hypothesis, we performed electrochemical experiments and extended this cryo-TEM analysis to four other electrolytes with a variety of salts, solvents, and additives from the literature: 1 M $LiPF_6$ in EC/DEC with 10% fluoroethylene carbonate (EC/DEC, 10% FEC), 1 M lithium bis(fluorosulfonyl)imide (LiFSI) in 1,2-dimethoxyethane (DME), 4 M LiFSI in DME, and 1 M LiFSI in fluorinated 1,4-dimethoxylbutane (FDMB) (*7*). These electrolytes have different Coulombic efficiencies (CEs) measured with the Aurbach method, ranging from 97.2 to 99.4%. Despite their differences in surface tension and viscosity, we could obtain high-quality thin film vitrified specimens for all

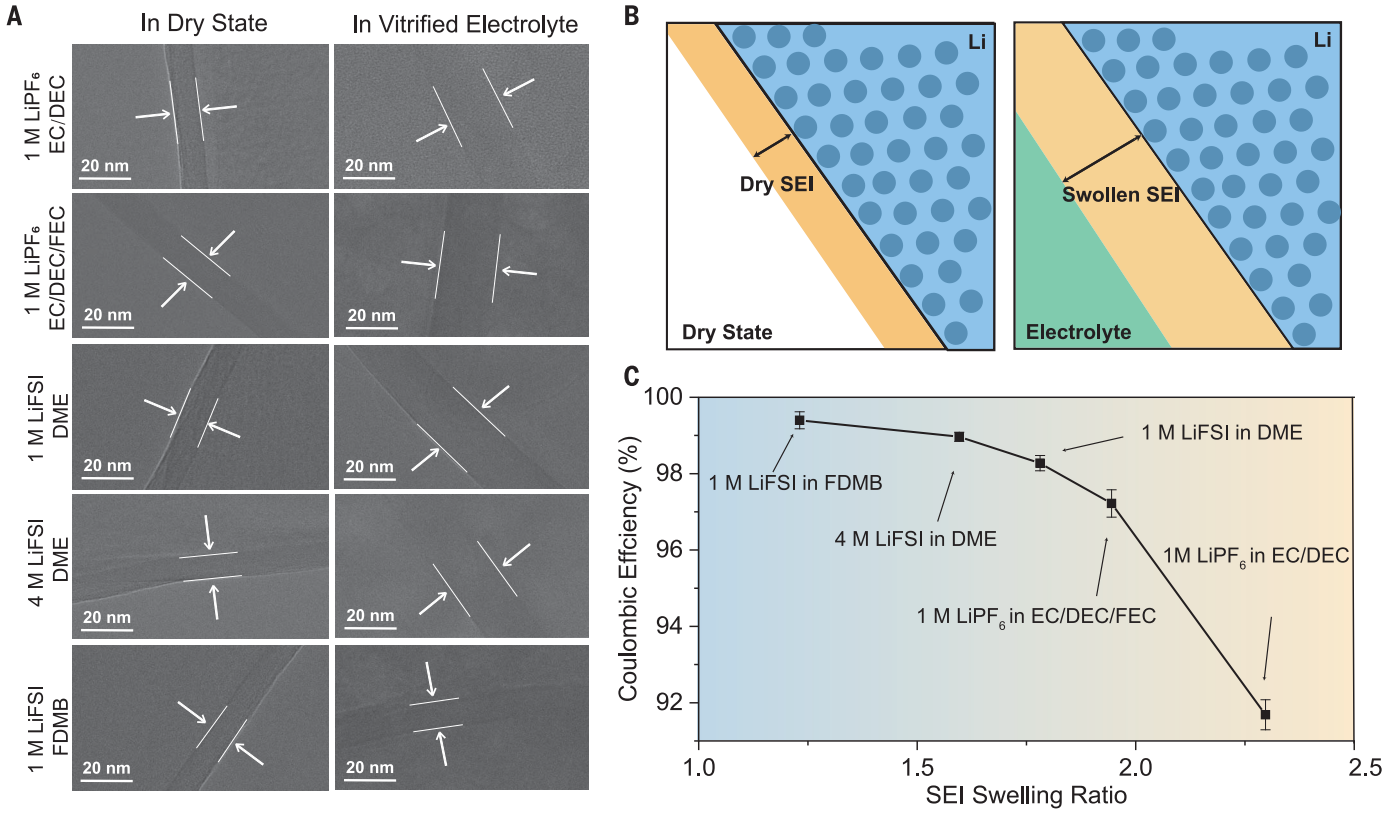

Fig. 4. The correlation of Li metal anode performance and swelling ratio of SEI in different electrolytes. (**A**) Representative comparison of SEI thickness in d-SEI and w-SEI with high-resolution cryo-TEM for various electrolyte systems. (**B**) d-SEI is thinner compared with w-SEI in vitrified electrolyte for all five systems. (**C**) SEI swelling ratio (w-SEI thickness versus d-SEI thickness) as a function of CE.

these electrolytes (fig. S7). No salt precipitation was observed even for the highly concentrated electrolyte (fig. S8).

We find the swelling of SEI in the electrolyte to be a universal phenomenon across all these electrolyte systems, regardless of solvent chemistry (Fig. 4 and table S1). This swelling behavior is dependent on electrolyte chemistry and highly correlated to battery performance, where higher degrees of SEI swelling tend to exhibit poor electrochemical cycling. The average d-SEI thicknesses in these five electrolytes are 8.8, 10.2, 9.9, 9.8, and 8.8 nm, whereas the average thicknesses of corresponding w-SEI are 20.1, 19.8, 17.6, 15.7, and 10.9 nm, respectively (fig. S9 and table S1). We correlate the cycling performance of Li metal anode represented by CE with SEI swelling behaviors. Among the five electrolytes examined here, 1 M $LiPF_6$ in EC/DEC—the electrolyte with the lowest CE or worst cycling performance—has the largest swelling ratio, ~2.3. For one of the best performing electrolytes, 1 M LiFSI in FDMB, this ratio is the smallest, ~1.2. Overall, an increased swelling ratio correlates to a decreased CE (i.e., cycle life) (table S1).

We also find that the increase of elements associated with salt decomposition in d-SEI is accompanied by a decrease in swelling ratio. These elements most likely form inorganic domains in the SEI, and inorganic species in SEI have less affinity toward organic solvents compared with organic species. This results in a less–electrolyte-philic SEI with a smaller swelling ratio. In the 0.1 M $LiPF_6$ in EC/DEC electrolyte, where the salt concentration is much lower than that in commercial carbonate electrolytes, we observed a swelling ratio of ~2.6, which is higher than that of 1 M $LiPF_6$ in EC/DEC (fig. S10 and table S2). The elastic moduli of both d-SEI and w-SEI are lower than those of 1 M $LiPF_6$ in EC/DEC, respectively (fig. S11), corresponding to a more polymeric composition, as expected. Such analysis is also valid in ether-based electrolytes (table S3). The highly concentrated electrolyte, 4 M LiFSI in DME, exhibited a smaller swelling ratio as well as a higher elastic modulus for both d-SEI and w-SEI compared with 1 M LiFSI in DME (fig. S12), in accord with the account that SEI from 4 M LiFSI in DME is highly anion derived (*9*). Such observation of smaller swelling ratios in more–inorganic-rich SEI provides a possible explanation for the pursuit of more–anion-derived SEI in the community. The better anion-derived SEI has a higher ratio of elements from the decomposition products of the salt instead of solvents, which means that the SEI swells less with the electrolyte to remain mechanically robust and chemically passivating. This relationship between SEI swelling and battery performance can be a potential design principle in conjunction with other electrochemical and mechanical properties, such as ionic conductivity, elasticity, and uniformity. Because current density plays a critical role in controlling the structure of SEI (*33*), this analysis could be further extended to understand current density effect on SEI composition and nanostructure (fig. S13 and table S4). Beyond that, given the similarities in chemical composition of SEI, we also expect this swelling behavior in SEI on other negative electrodes. Furthermore, such insights also highlight the importance of preserving both the liquid and solid phases for studying complex interfacial phenomena with high resolution using cryo-EM methods.

REFERENCES AND NOTES

1. A. J. Bard *et al.*, *J. Phys. Chem.* **97**, 7147–7173 (1993).
2. V. R. Stamenkovic, D. Strmcnik, P. P. Lopes, N. M. Markovic, *Nat. Mater.* **16**, 57–69 (2017).
3. K. Xu, *Chem. Rev.* **114**, 11503–11618 (2014).
4. E. Peled, S. Menkin, *J. Electrochem. Soc.* **164**, A1703–A1719 (2017).
5. M. B. Pinson, M. Z. Bazant, *J. Electrochem. Soc.* **160**, A243–A250 (2013).
6. X. Cao *et al.*, *Nat. Energy* **4**, 796–805 (2019).
7. Z. Yu *et al.*, *Nat. Energy* **5**, 526–533 (2020).
8. R. Weber *et al.*, *Nat. Energy* **4**, 683–689 (2019).
9. J. Qian *et al.*, *Nat. Commun.* **6**, 6362 (2015).
10. M. Gauthier *et al.*, *J. Phys. Chem. Lett.* **6**, 4653–4672 (2015).
11. X. Yu, A. Manthiram, *Energy Environ. Sci.* **11**, 527–543 (2018).
12. X.-B. Cheng, R. Zhang, C.-Z. Zhao, Q. Zhang, *Chem. Rev.* **117**, 10403–10473 (2017).
13. J. W. Choi, D. Aurbach, *Nat. Rev. Mater.* **1**, 16013 (2016).
14. Y. Li *et al.*, *Science* **358**, 506–510 (2017).
15. X. Wang *et al.*, *Nano Lett.* **17**, 7606–7612 (2017).
16. W. Huang *et al.*, *Nano Lett.* **19**, 5140–5148 (2019).
17. W. Huang *et al.*, *Matter* **1**, 1232–1245 (2019).
18. Z. Zhang *et al.*, *Matter* **4**, 302–312 (2021).
19. M. J. Zachman, Z. Tu, S. Choudhury, L. A. Archer, L. F. Kourkoutis, *Nature* **560**, 345–349 (2018).
20. K. A. Taylor, R. M. Glaeser, *Science* **186**, 1036–1037 (1974).
21. D. Danino, R. Gupta, J. Satyavolu, Y. Talmon, *J. Colloid Interface Sci.* **249**, 180–186 (2002).
22. L. Wang *et al.*, *Nat. Chem.* **11**, 789–796 (2019).
23. M. Rubinstein, R. H. Colby, *Polymer Physics* (Oxford Univ. Press, 2003).
24. R. Subramani *et al.*, *Front. Mater.* **7**, 212 (2020).
25. S. Kranz, T. Kranz, A. G. Jaegermann, B. Roling, *J. Power Sources* **418**, 138–146 (2019).
26. M. Nojabaee, K. Küster, U. Starke, J. Popovic, J. Maier, *Small* **16**, e2000756 (2020).
27. F. Single, B. Horstmann, A. Latz, *Phys. Chem. Chem. Phys.* **18**, 17810–17814 (2016).
28. M. Garreau, *J. Power Sources* **20**, 9–17 (1987).
29. P. Guan, L. Liu, X. Lin, *J. Electrochem. Soc.* **162**, A1798–A1808 (2015).
30. J. Popovic, *Energy Technol.* **9**, 2001056 (2021).
31. X. Ren *et al.*, *Proc. Natl. Acad. Sci. U.S.A.* **117**, 28603–28613 (2020).
32. X.-B. Cheng *et al.*, *Adv. Sci.* **3**, 1500213 (2016).
33. Y. Xu *et al.*, *ACS Nano* **14**, 8766–8775 (2020).

ACKNOWLEDGMENTS

We acknowledge the use and support of the Stanford-SLAC Cryo-EM Facilities. Part of this work was performed at the Stanford Nano Shared Facilities (SNSF) and the Stanford Nanofabrication Facility (SNF). K3 IS camera and support are courtesy of Gatan, Inc. **Funding:** This study received funding from the Office of Basic Energy Sciences, Division of Materials Science and Engineering, Department of Energy, DE-AC02-76SF00515 (to Y.C. and W.C.); the Stanford Interdisciplinary Graduate Fellowship (to Z.Z. and W.Z.); the Stanford University Knight Hennessy scholarship (to S.T.O.); and National Science Foundation award ECCS-2026822. **Author contributions:** Z.Z., Yu.L., W.C., and Y.C. conceived the project and designed the experiments. Z.Z. performed electrochemical measurements. Z.Z. carried out cryo-(S)TEM experiments. Yu.L. helped with cryo-TEM experiments. R.X. and Z.Z. designed and carried out AFM measurements. W.Z. performed cryo-SEM characterization. Ya.L. and Y.W. helped with TEM grid modification. Z.Y. and Z.B. synthesized and provided the FDMB electrolyte. S.T.O., J.X., H.W., W.H., D.T.B., Ya.L., Y.Y., J.W., and H.C. interpreted the TEM and electrochemical data. Z.Z., W.C., and Y.C. cowrote the manuscript. All authors discussed the results and commented on the manuscript. **Competing interests:** The authors declare that they have no competing interests. **Data and materials availability:** All data needed to evaluate the conclusions in this paper are present in the paper or the supplementary materials.

SUPPLEMENTARY MATERIALS

science.org/doi/10.1126/science.abi8703
Materials and Methods
Figs. S1 to S13
Tables S1 to S4
References (*34*–*38*)
Movies S1 and S2

6 April 2021; accepted 10 November 2021
10.1126/science.abi8703

Science

Capturing the swelling of solid-electrolyte interphase in lithium metal batteries

Zewen ZhangYuzhang LiRong XuWeijiang ZhouYanbin LiSolomon T. OyakhireYecun WuJinwei XuHansen WangZhiao YuDavid T. BoyleWilliam HuangYusheng YeHao ChenJiayu WanZhenan BaoWah ChiuYi Cui

Science, 375 (6576), • DOI: 10.1126/science.abi8703

Preservation of cycling behavior

Understanding the changes in interfaces between electrode and electrolyte during battery cycling, including the formation of the solid-electrolyte interphase (SEI), is key to the development of longer lasting batteries. Z. Zhang *et al*. adapt a thin-film vitrification method to ensure the preservation of liquid electrolyte so that the samples taken for analysis using microscopy and spectroscopy better reflect the state of the battery during operation. A key finding is that the SEI is in a swollen state, in contrast to current belief that it only contained solid inorganic species and polymers. The extent of swelling can affect transport through the SEI, which thickens with time, and thus might also decrease the amount of free electrolyte available for battery cycling. —MSL

Science (ISSN) is published by the American Association for the Advancement of Science. 1200 New York Avenue NW, Washington, DC 20005. The title *Science* is a registered trademark of AAAS.